How to cite: *Angew. Chem. Int. Ed.* **2020**, *59*, 22382–22387
International Edition: doi.org/10.1002/anie.202006135
German Edition: doi.org/10.1002/ange.202006135

Intermetallics

Exotic Compositional Ordering in Manganese–Nickel–Arsenic (Mn-Ni-As) Intermetallics

*Bruno Gonano, Øystein Slagtern Fjellvåg, Gwladys Steciuk, Dipankar Saha, Denis Pelloquin, and Helmer Fjellvåg**

Abstract: *In this work we benefited from recent advances in tools for crystal-structure analysis that enabled us to describe an exotic nanoscale phenomenon in structural chemistry. The $Mn_{0.60}Ni_{0.40}As$ sample of the $Mn_{1-x}Ni_xAs$ solid solution, exhibits an incommensurate compositional modulation intimately coupled with positional modulations. The average structure is of the simple NiAs type, but in contrast to a normal solid solution, we observe that manganese and nickel segregate periodically at the nano-level into ordered MnAs and NiAs layers with thickness of 2–4 face-shared octahedra. The detailed description was obtained by combination of 3D electron diffraction, scanning transmission electron microscopy, and neutron diffraction. The distribution of the manganese and nickel layers is perfectly described by a modulation vector $q = 0.360(3)\ c^*$. Displacive modulations are observed for all elements as a consequence of the occupational modulation, and as a means to achieve acceptable Ni–As and Mn–As distances. This modulated evolution of magnetic MnAs and non-magnetic NiAs-layers with periodicity at approximately 10 Å level, may provide an avenue for spintronics.*

Since the discovery of X-rays, scientists have studied atomic arrangements in solids considering their intrinsic beauty and their role as the active link between atoms and physical properties of materials. In a crystal structure, one finds different sites for cations and anions, reflecting their different chemical properties (i.e. size, charge, electronegativity, etc.). This gives rise to a huge range of crystal structure types, from simple to very complex ones among proteins, organic and inorganic compounds.

Incommensurately modulated crystal structures with their high complexity, attract a lot of interest in solid-state science. Both occupancy and position can be modulated. The modulation can originate from a wide variety of structural perturbations like incommensurate oxygen vacancies ordering,[1] polyhedral distortions[2,3] and compositional ordering.[4] Incommensurate modulations are quite well understood in oxides while intermetallics present a challenge in terms of structural analysis.[5–7]

An incommensurate partial cation occupancy modulation has been reported for $LaNb_{0.88}W_{0.12}O_{4.06}$.[8] This compound has a modulation linked to a preferential cation nano-segregation of tungsten atoms. In intermetallics, positional modulation has been observed in different compounds, for example, in the Nowotny Chimney-ladder phases,[9–11] that can described as an intertwining between two sublattices. Similar phenomena are present in $Cu_{3+x}Si$,[12] which displays a very complex incommensurate modulation and illustrate well the complexity in disclosing structural details for such systems.

Ferromagnetic MnAs (space group $P6_3/mmc$) is an example of a simple crystal structure derived from ABAB sphere packing of As, with Mn in octahedral sites formed by closed-packed As-layers, giving rise to face-sharing chains of $MnAs_6$-octahedra along [001] with two octahedra per unit cell. In the *ab*-plane, the $MnAs_6$-octahedra are edge-sharing. Pauli paramagnetic NiAs (space group $P6_3/mmc$) adopts the same structure type, but with different unit cell parameters (due to the different size of Mn and Ni).

The intermediate solid solution between MnAs and NiAs, $Mn_{1-x}Ni_xAs$ $(0 \le x \le 1)$, was investigated in the 1980s and revealed an unsolved structural phenomenon for $0.25 \le x \le 0.75$.[13] A possible modulation due to Ni ordering was proposed, but no available technique could confirm or invalidate this speculation. Therefore, the question of a Mn-Ni-ordering in $Mn_{1-x}Ni_xAs$ remained unanswered. Today, state-of-the-art analytical tools have evolved to the point that revisiting this system can provide answers. We here reveal an exotic Mn-Ni-ordering in $Mn_{0.60}Ni_{0.40}As$, which appears to represent a phenomenon not earlier observed.

Initially, we studied the lattice of $Mn_{0.60}Ni_{0.40}As$ by conventional electron diffraction (ED), and the data revealed an expected complex unit cell. Electron diffraction pattern of the [100]-zone axis shows additional reflections (Figure 1 a) that can be indexed by an incommensurate modulation vector ($\boldsymbol{q} = 0.36\,\boldsymbol{c}^*$), confirming the presence of additional order in

[*] B. Gonano, D. Saha, H. Fjellvåg
Center for Materials Science and Nanotechnology, Department of Chemistry, University of Oslo
P.O. Box 1033 Blindern, 0315 Oslo (Norway)
E-mail: helmer.fjellvag@kjemi.uio.no
Ø. S. Fjellvåg
Department for Neutron Materials Characterization, Institute for Energy Technology
PO Box 40, 2027 Kjeller (Norway)
G. Steciuk
Institute of Physics, Academy of Sciences of the Czech Republic
v.v.i, Na Slovance 2, 18221 Prague (Czech Republic)
D. Pelloquin
Laboratoire CRISMAT, UMR 6508 CNRS ENSICAEN
6 bd du Maréchal Juin, 14050 Caen Cedex 4 (France)
Supporting information and the ORCID identification number(s) for the author(s) of this article can be found under: https://doi.org/10.1002/anie.202006135.

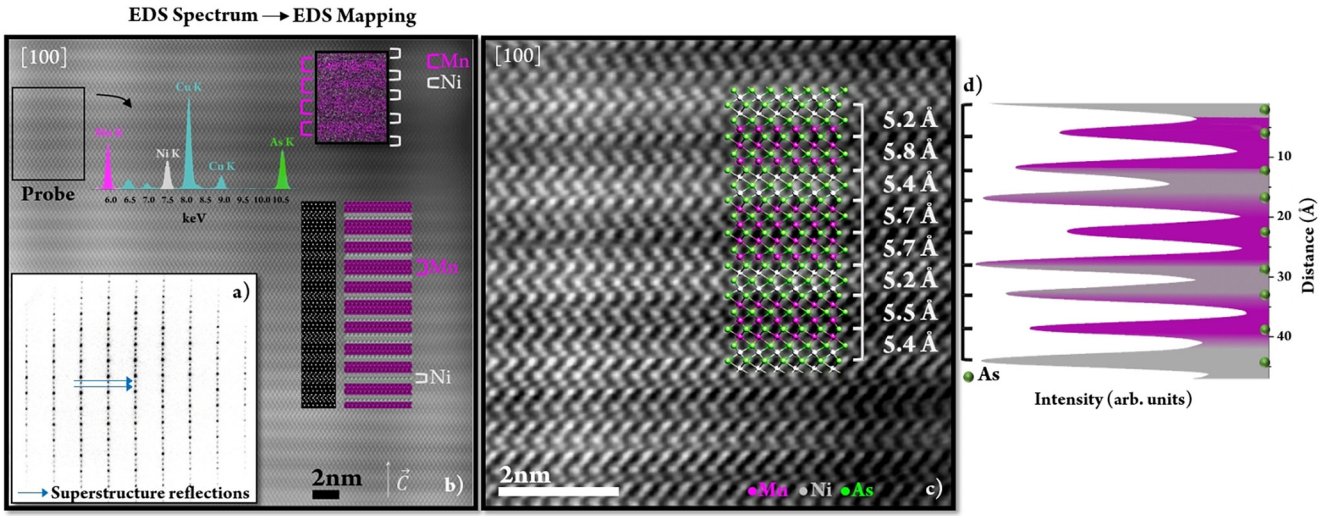

Figure 1. a) Electron diffraction of the [100]-zone axis of $Mn_{0.60}Ni_{0.40}As$ showing satellite reflections, corresponding to an incommensurate modulation vector along c^* ($q = 0.36\,c^*$); b) Experimental [100] HAADF image of $Mn_{0.60}Ni_{0.4}As$ (magnification x8M). Bright dots are related to As rows while darker and brighter layers represent MnAs and NiAs, respectively. On the right side, simulated image confirms the goodness of the structural model. The structural model is shown beside. Top left inset: EDS spectrum related to recorded zone (probe) identified by a black box. Top right inset: EDS mapping evidencing richer zones in Mn (purple) and Ni (grey); c) Experimental [100] HAADF image of $Mn_{0.60}Ni_{0.4}As$ (magnification x25M) showing variations in distances between As atoms from Mn (darker) and Ni (brighter) layers. A snapshot of the structural model is inserted; d) Intensity line profile extracted from the HAADF image along [001], displaying the variations of As-As distances in the MnAs and NiAs layers.

the compound. The corresponding High-Angle Annular Dark Field (HAADF) image coupled with local EDX collections yields good elemental contrasts correlated to Mn and Ni species and reveals two types of layers perpendicular to the modulation vector [001] (Figure 1 b and c). We interpret these images as a specific ordering between Mn and Ni based layers, as supported by energy-dispersive X-ray spectroscopy mapping (EDX) (Figure 1 b).

The thickness of these layers can be measured in terms of the number of connected octahedra, being 3–4 for the MnAs and 2–3 for the NiAs slabs of the integrated structure. This creates a unique nanolayered structure, with the compositional modulation being a genuine part of the crystal structure of the phase. We note that the layers appear to be fully occupied by either Mn or Ni, indicating that the ordering is complete.

Careful analysis of the As-As distances along [001] in the x25M HAADF image, reveals a distinct difference between the zones richer in Mn or in Ni (Figure 1 c). Whereas for the brighter layer (Ni-rich) the As-As distance tends to be shorter, it increases in the darker Mn-rich regions, according to the longer *c*-axis of MnAs (5.8 Å) compared to that of NiAs (5.0 Å). This is supported by the extracted line profile for the As-As distances in Figure 1 d.

At this point, it is clear that the Mn-Ni ordering is real. We now use 3D ED to unveil a structural model.[14] This technique has recently proved his ability to yield valid structural models in complex systems[15] and provide single-crystal diffraction data on small areas of few hundreds of nanometers, also on powder samples. It must be mentioned here that 3D ED represents a broad range of experimental protocols and that this study refers to Precession Electron Diffraction Tomography (PEDT).

3D ED shows the expected hexagonal subcell, but also additional reflections at incommensurate positions (Figure 2 a). The reciprocal space was indexed using the super-

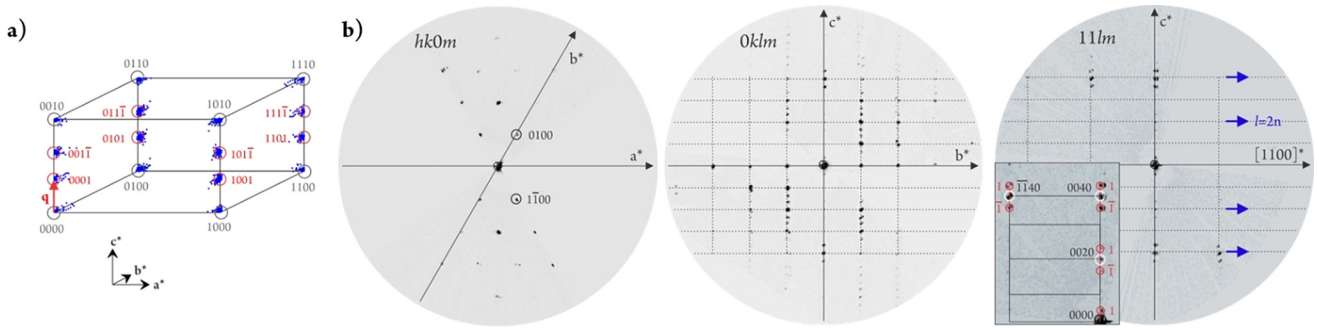

Figure 2. a) Reciprocal space projected in one-unit cell showing satellite reflections up to first order (red); b) Sections of reciprocal space from PEDT data.

space formalism considering a hexagonal unit cell: $a = 3.653(8)$ Å, $c = 5.417(3)$ Å and with a modulation vector $\boldsymbol{q} = 0.360(3)\boldsymbol{c}^*$ to index satellite reflections up to first order. As expected from the conventional ED, the modulation is incommensurate. The volume of the average unit cell ($V = 62.67$ Å^3) is in between the volumes of NiAs ($V = 56.7$ Å^3) and MnAs ($V = 68.55$ Å^3).[16,17] Information on symmetry is obtained from for example, the sections 11 lm and 0*klm* of the reciprocal space for which the extinction conditions $l = 2n$ on 00*l* and 11*lm* are characteristic of a 6_3-screw axis along [001] and a *c*-glide mirror perpendicular to [1−10], respectively (Figure 2b). These conditions are compatible with two superspace groups (SSG); $P6_3/mmc(00\gamma)0000$ and $P6_3mc(00\gamma)000$. The structure was solved from the 3D ED data in SSG $P6_3/mmc(00\gamma)0000$ with $\boldsymbol{q} = 0.360(3)\boldsymbol{c}^*$ and a data coverage of 100% for 0.7 Å^{-1}resolution shell. Our subsequent refinements indicated that the structure is centrosymmetric $P6_3/mmc(00\gamma)0000$.

The initial solution obtained by charge flipping algorithm is a 3D map of the electrostatic potential (e-map) represented as isosurfaces (Figure 3a).

First, the average framework of (Mn, Ni)As_6 octahedra is revealed in agreement with the initially reported structure.[13] The model is further elaborated by calculating de Wolf sections *x3-x4* around the two atomic sites corresponding to Mn/Ni and As atoms (Figure 3b). The As site exhibits a displacive modulation along *c*, described using a continuous harmonic function. In order to account for the Mn/Ni ordering along [001], the site shared by Mn and Ni atoms is split using discontinuous crenel-like functions associated with one harmonic function.[18] Within the resolution of the 3D ED data, the electron scattering amplitudes for Mn and Ni are too

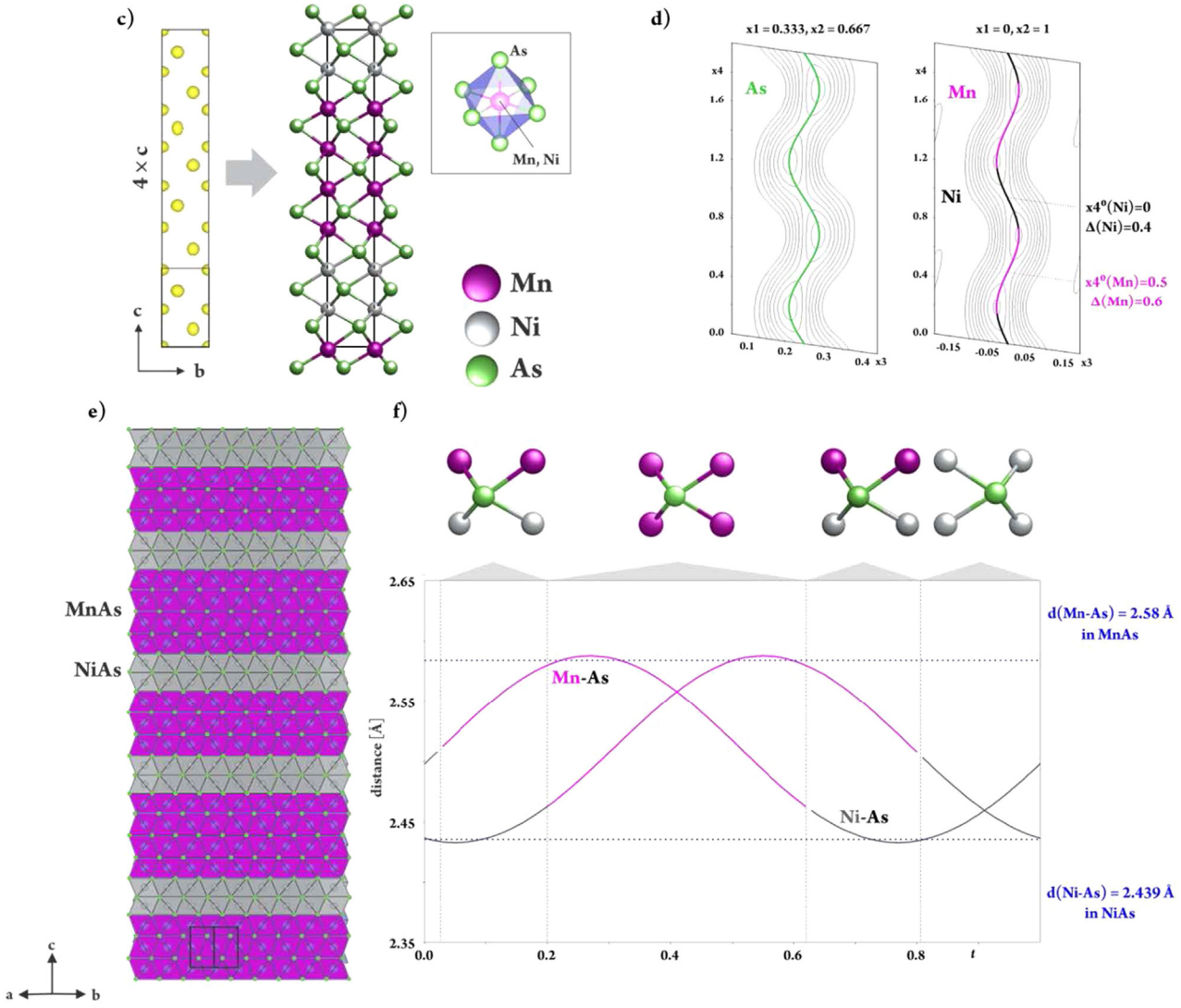

Figure 3. a) [100] projection of the 3D electronic potential map and its interpretation as a structural model. For better visualization of the layers, the model is extended along the stacking direction.[001] The Mn and Ni cations are in octahedral coordination; b) On the De Wolf section *x3−x4* calculated around the As site, the cationic site is described with a continuous harmonic function and split between 2 sites for Mn and Ni using discontinuous crenel-like functions; c) Extended [110] projection of the refined structure against PEDT data (dynamical refinement); d) Variation in Mn–As and Ni–As distances showing the evolution of the local As environment as function of the modulation.

close to reliably detect a difference in the electrostatic potential between the domains.

For this reason, the centers of the crenels are set to $x4^0(\mathrm{Mn}) = 0.5$ and $x4^0(\mathrm{Ni}) = 0$ in order to strain the shortest (longest) distances for Ni-As (Mn-As). The crenel widths were set according to the composition: $\Delta(\mathrm{Mn}) = 0.6$ and $\Delta(\mathrm{Ni}) = 0.4$ (Figure 3b). For better visualization of the Mn-Ni stacking sequence, the e-map, as well as the interpreted model, is represented in an averaged supercell $a \times b \times 4c$. The main experimental parameters are listed in Table 1 (SI).

The model exhibits the alternation of two types of blocks with variable thickness consisting either of layers of $MnAs_6$ octahedra or of layers of $NiAs_6$ octahedra. Dynamical refinements were carried out against the 3D ED data.[10,11] The included reflections were chosen following the recommendation by Palatinus et al.[19,20] $RSg(\mathrm{max}) = 0.9$, S(max)g-(matrix) = 0.01 Å^{-1}, g(max) = 1.7 Å^{-1}. Because of the rather small unit cell volume and the high symmetry, the $RSg(\mathrm{max})$ was set to a high value to thereby include a sufficiently large number of reflections and maintain a good reflection-to-parameter ratio (Table 1 (SI)). The refinement gave reliability factors of $R/wR(\mathrm{obs/all}) = 13.85\,\%/14.65\,\%$ for N obs/all = 796/1788 [main: $R/wR(\mathrm{obs}) = 12.67\,\%/14.28\,\%$; 1. order: $R/wR(\mathrm{obs}) = 16.24\,\%/15.75\,\%$].

This represent a huge improvement compared to what offered in a kinematical refinement [$R/wR(\mathrm{obs/all}) = 30.18\,\%/35.39\,\%$ for N obs/all = 88/128].

The crystal structure of $Mn_{0.60}Ni_{0.40}As$ exhibits an alternation of 3–4 layers of MnAs and 2–3 layers of NiAs (Figure 3c), described by a genuine incommensurate modulation with respect to the chemical composition. As shown by Fjellvåg et al.[13] the $Mn_{0.60}Ni_{0.40}As$ sample represents just an arbitrary composition for the $Mn_{1-x}Ni_xAs$ solid solution where superstructure peaks are observed. The simulated HAADF image (calculated by JEMS software) based on the aforementioned incommensurate structure model is included in Figure 1b and shows very good compliance with the observed image. The observed positional modulation of the Mn, Ni and As atoms along [001] dictates a difference in the cell volume for the MnAs and NiAs layers, being in agreement with unit cell volumes of the binary compounds as well as the HAADF images.

The expected Mn-As and Ni-As bond lengths are reached owing to the displacive modulations of As and Mn/Ni along the stacking direction c (Figure 3d). This information corroborates our initial observations from HAADF imaging (Figure 1b and c).

The collected powder neutron diffraction (PND) pattern shows intense reflections at low scattering angle (Figure 4), for example, at 0.42 Å^{-1}, which is a first-order satellite reflection from the compositional modulation of Mn and Ni. The strong signal of the satellite reflections is a consequence of the excellent contrast between Mn and Ni in PND, due to the different signs of their scattering lengths.

Thus, unlike what was feasible with 3D ED data, the sample composition can be determined with accuracy by Rietveld refinement of the crenel widths from PND data. The derived composition of $Mn_{0.598(3)}Ni_{0.402(7)}As$ is in line with the nominal composition from synthesis.

The modulation vector obtained from the PND Rietveld refinements [$\boldsymbol{q} = 0.3594(2)\,\boldsymbol{c}^*$] is identical to that obtained by 3D ED [$\boldsymbol{q} = 0.360(3)\,\boldsymbol{c}^*$]. We note that the results obtained from refinements of PND and 3D ED data are identical, within statistical uncertainty. We emphasize that the combination of PND and 3D ED data was necessary to fully understand the structure as PND is superior for refining the exact composition, while 3D ED was needed for structural determination. The final refined structural model from both data sets is presented in Table 1 and Table 2.

The type of intrinsic "nano-layering" observed for $Mn_{0.60}Ni_{0.40}As$ is unique. There exist a few examples of related features. It is reminiscent of the layered ferecrystals that can be described as an intergrowth between two different types of cation—anion layers, bonded by weak Van der Walls forces (e.g. m bilayers of SnSe and one trilayer of $NbSe_2$, $[(SnSe)_{1+\gamma}]_m(NbSe_2)_1$). However, ferecrystals clearly differ from $Mn_{0.60}Ni_{0.40}As$ by being constructed of weakly bonded building bricks that furthermore can exist as independent well defined compounds.

The present phenomenon is unlike that of other modulated compounds. The layers in the $Mn_{0.60}Ni_{0.40}As$ compound

Table 1: Unit-cells parameters extracted from refinement of 3D ED data and neutron diffraction data.

Structural formula	$AsMn_{0.6}Ni_{0.4}$
Unit-cell parameters (PEDT)	$a = 3.653(8)$ Å, $c = 5.417(3)$ Å, $\gamma = 120°$, $\boldsymbol{q} = 0.360(3)\,\boldsymbol{c}^*$, $V = 62.67$ Å^3
Unit-cell parameters (NPD)	$a = 3.6520(2)$ Å, $c = 5.4280(6)$ Å, $\gamma = 120°$, $\boldsymbol{q} = 0.3594(2)\,\boldsymbol{c}^*$, $V = 62.694(6)$ Å^3
Z	2
Density [g cm^{-3}] (from NPD)	6.96(7)
Space group	$P6_3/mmc$

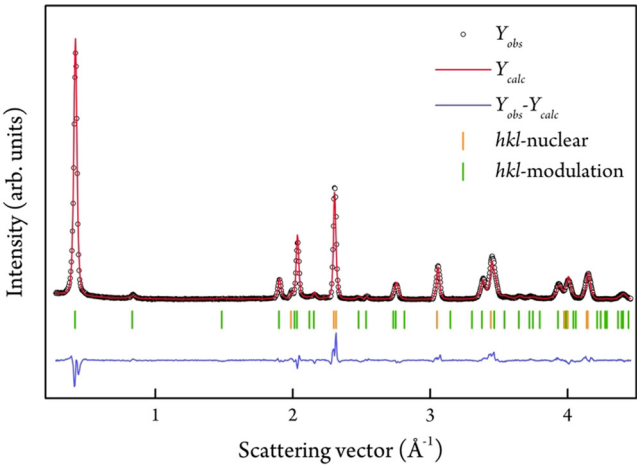

Figure 4. Experimental (black circles), calculated (red line) and difference (blue line) neutron powder diffraction pattern of $Mn_{0.60}Ni_{0.40}As$ according to Rietveld refinement. Main and satellite Bragg peak positions are indicated with green and orange sticks, respectively.

Table 2: Positional parameters extracted from the dynamical refinement of 3D ED data and neutron diffraction data.

Dynamical refinement against 3D ED data						
atom	Δ/Occ.	harm.	*x*/*a*	*y*/*b*	*z*/*c*	*U*iso [Å^2]
Mn1	0.6		0	1	0	0.0191(9)
		s,1	0	0	−0.0313(6)	
Ni1	0.4		0	1	0	0.0191(9)
		s,1	0	0	−0.0313(6)	
As1	1		0.3333	0.6667	0.25	0.0215(9)
		s,1	0	0	−0.0468(6)	
Refined positional parameters (powder neutron)						
Mn1	0.598(3)	s,1	0	0	−0.003(3)	0.016(1)
Ni1	0.402(3)	s,1	0	0	−0.003(3)	0.016(1)
As1	1	s,1	0	0	−0.037(1)	0.005

are of the same crystal structure, in contrast to the Nowotny Chimney-ladder phases. In compounds like $Cu_{3+x}Si$, the modulation is positional and is not originating from an ordering between Cu and Si atoms.

The oxide $LaNb_{0.88}W_{0.12}O_{4.06}$ has certain similarities to $Mn_{0.60}Ni_{0.40}As$ by being occupationally modulated. However, there are significant differences: (i) only occupational modulation is observed, while $Mn_{0.60}Ni_{0.40}As$ exhibits both occupational and positional modulation; (ii) the occupational modulation of Mn and Ni in $Mn_{0.60}Ni_{0.40}As$ leads to a complete segregation into MnAs and NiAs regions, whereas $LaNb_{0.88}W_{0.12}O_{4.06}$ only shows partial segregation of W; (iii) the architecture of the segregation itself differs; 2D layers versus 3D network, and (iv) the bonding in the two cases is very different; metallic versus polar covalent/ionic. Last, we note that MnAs is ferromagnetic and NiAs is paramagnetic, which makes the intrinsically nanolayered material a potential candidate for spintronics.

$Mn_{0.60}Ni_{0.40}As$ is, to our knowledge, the first example of a representative of a solid solution compound where the chemical composition is directly reflected in an occupational modulation that is intimately coupled to a positional modulation. It is surprising that this exotic and unique phenomenon with Mn-Ni occupational modulation occurs for a phase ideally taking the simple NiAs-type structure. We stress that this modulation of composition, materialized by ultrathin layers consisting of edge- and face- sharing Mn-As octahedra and of Ni-As octahedra, is different from any other stacking or order/disorder phenomena.

The modulated structure is the genuine crystal structure of $Mn_{0.60}Ni_{0.40}As$. The periodic variation in the stacking of 2D layers of MnAs and NiAs, creates an incommensurate modulation, with 3–4 thick layers of MnAs and 2–3 layers of NiAs, that in turn determines the chemical composition of the material. In this work, we show how the structural model to describe this peculiar phenomenon can be derived from 3D ED and validated by refinement of powder neutron diffraction data with excellent Mn/Ni scattering contrast. The refined composition is in full compliance with the nominal composition from synthesis. The structure model, as well as the coupled HAADF-EDS mapping images, shows that the MnAs layers have a longer *c*-axis than the NiAs layers, in full agreement with crystallographic data for the individual binary compounds.

We have demonstrated the existence of a fascinating nanophenomenon in a solid-solution phase, and the ability, strength and robustness of state-of-the-art tools in crystallography and methodology to solve and describe complex incommensurate phenomena, all acting as inspiration for future research. The modulated feature of strongly magnetic MnAs and non-magnetic NiAs layers with periodic layer thicknesses at the 1 nm scale, is likely to attract attention in fields like spintronics.

Acknowledgements

This work is part of the activities of the NAMM project (Novel Approaches to Magneto-Structural phases transitions in Metallic systems), supported by the Research Council of Norway (Grant no. 263241). Authors want to acknowledge Susmit Kumar, Center for Materials Science and Nanotechnology, Department of Chemistry, University of Oslo for fruitful discussions. The authors acknowledge Vivian Nassif, Inès Puente-Orench and the staff at the D1B beamline, ILL, France, for beamtime allocation and technical support. (S)TEM experiments have been performed in the CRISMAT Lab. (UMR6508, Caen, France) within the frame of the METSA federation (FR3507). G.S. acknowledges the Czech Science Foundation through Project No. 19-07931Y.

Conflict of interest

The authors declare no conflict of interest.

Keywords: electron diffraction · intermetallics · neutron diffraction · solid-state structures

[1] J. D. C. McConnell, V. Heine, *Phys. Rev. B* **1985**, *31*, 6140 – 6142.
[2] C. J. Howard, M. A. Carpenter, *Acta Crystallogr. Sect. B* **2010**, *66*, 40 – 50.
[3] L. J. Gillie, J. Hadermann, O. Pérez, C. Martin, M. Hervieu, E. Suard, *J. Solid State Chem.* **2004**, *177*, 3383 – 3391.
[4] L. Norén, R. L. Withers, R. Berger, *J. Solid State Chem.* **2000**, *151*, 260 – 266.
[5] M. Boström, S. Lidin, *J. Alloys Compd.* **2004**, *376*, 49 – 57.
[6] H. Lind, M. Boström, V. Petříček, S. Lidin, *Acta Crystallogr. Sect. B* **2003**, *59*, 720 – 729.
[7] S. Y. Piao, L. Palatinus, S. Lidin, *Inorg. Chem.* **2008**, *47*, 1079 – 1086.
[8] C. Li, S. S. Pramana, S. J. Skinner, *Dalton Trans.* **2019**, *48*, 1633 – 1646.
[9] D. C. Fredrickson, S. Lee, R. Hoffmann, *Inorg. Chem.* **2004**, *43*, 6159 – 6167.

[10] N. Sato, H. Ouchi, Y. Takagiwa, K. Kimura, *Chem. Mater.* **2016**, *28*, 529 – 533.
[11] F. E. Rohrer, H. Lind, L. Eriksson, A.-K. Larsson, S. Lidin, *Z. Kristallogr. - Cryst. Mater.* **2001**, *216*, 190 – 198.
[12] L. Palatinus, M. Klementová, V. Dřínek, M. Jarošová, V. Petříček, *Inorg. Chem.* **2011**, *50*, 3743 – 3751.
[13] H. Fjellvåg, A. Kjekshus, A. Andresen, A. Ziéba, *J. Magn. Magn. Mater.* **1986**, *61*, 61 – 80.
[14] M. Gemmi, E. Mugnaioli, T. E. Gorelik, U. Kolb, L. Palatinus, P. Boullay, S. Hovmöller, J. P. Abrahams, *ACS Cent. Sci.* **2019**, *5*, 1315 – 1329.
[15] G. Steciuk, L. Palatinus, J. Rohlíček, S. Ouhenia, D. Chateigner, *Sci. Rep.* **2019**, *9*, 9156.
[16] N. Alsén, *Geol. Foeren. Stockholm Foerh.* **1925**, *47*, 19 – 72.
[17] R. Wilson, J. Kasper, *Acta Crystallogr.* **1964**, *17*, 95 – 101.
[18] V. Petříček, V. Eigner, M. Dušek, A. Čejchan, *Z. Kristallogr. - Cryst. Mater.* **2016**, *231*, 301 – 312.
[19] L. Palatinus, V. Petříček, C. A. Corrêa, *Acta Crystallogr. Sect. A* **2015**, *71*, 235 – 244.
[20] L. Palatinus, C. A. Corrêa, G. Steciuk, D. Jacob, P. Roussel, P. Boullay, M. Klementová, M. Gemmi, J. Kopeček, M. C. Domeneghetti, F. Cámara, V. Petříček, *Acta Crystallogr. Sect. B* **2015**, *71*, 740 – 751.

Manuscript received: April 28, 2020
Accepted manuscript online: August 18, 2020
Version of record online: October 13, 2020

